buildings

MDPI

Article

Mechanical Performance of Hybrid Fibre Reinforced Magnesium Oxychloride Cement-Based Composites at Ambient and Elevated Temperature

Sanket Rawat, Paul Saliba, Peter Charles Estephan, Farhan Ahmad and Yixia Zhang *

School of Engineering, Design and Built Environment, Kingswood Campus, Western Sydney University, Sydney, NSW 2751, Australia
* Correspondence: sarah.zhang@westernsydney.edu.au

Abstract: Magnesium oxychloride cement (MOC) is often recognized as an eco-friendly cement and has found widespread application in various sectors. However, research on its resistance against elevated temperatures including fire is very limited. This paper thoroughly investigated the mechanical performance of fibre reinforced MOC-based cementitious composite (FRMOCC) at ambient and elevated temperatures. A recently developed water-resistant MOC was used as the base matrix which was further reinforced using hybrid basalt and polypropylene fibres at various proportions, and a systematic study on the effect of fibre dosage on compressive and tensile strength of FRMOCC was conducted. The specimens were exposed to elevated temperatures ranging from 200 to 800 °C; mechanical performance and phase composition from a microscale study were analysed. The findings revealed that compressive strength, with the increase in temperature, substantially decreased, with values of 30–87% at 400 °C and over 95% at 800 °C. Specimens with 1.5% basalt and 0.5% PP fibre showed the least reduction possibly due to the vacant channels created as a result of the melting effect of PP fibres. Tensile strength was also completely lost at 600 °C and the specimens suffered substantial mass loss exceeding 30% at this temperature, indicating significant matrix decomposition. Additional analysis using X-ray diffraction (XRD) and scanning electron microscope (SEM) revealed the decomposition stages of the matrix and highlighted the instability of the main hydration phases of FRMOCC at elevated temperatures.

Keywords: compressive strength; elevated temperature; fibre reinforced cementitious composites; hybrid fibre; magnesium oxychloride cement (MOC); tensile strength

Citation: Rawat, S.; Saliba, P.; Estephan, P.C.; Ahmad, F.; Zhang, Y. Mechanical Performance of Hybrid Fibre Reinforced Magnesium Oxychloride Cement-Based Composites at Ambient and Elevated Temperature. *Buildings* **2024**, *14*, 270. https://doi.org/10.3390/buildings14010270

Academic Editor: Łukasz Sadowski

Received: 18 December 2023
Revised: 10 January 2024
Accepted: 17 January 2024
Published: 19 January 2024

1. Introduction

Fire resistance is one of the important criteria in the design of any civil engineering structures and infrastructures. Multiple factors such as the type of material, heat intensity, duration of fire and exposure area collectively determine the severity of the damage, making it a very complex phenomenon. To minimize the risk of fire-induced damage, a practical approach involves utilizing fire-resistant construction and building materials for both structural and non-structural components, such as cladding panels. Recent incidents have shown that building fires have a high chance of originating from the cladding due to combustion of the cladding materials widely used in the market [1]. Use of certain types of cladding materials leads to the spread of fire, posing risks to occupants and firefighters. Numerous fire incidents involving combustible external composite panels, such as the 2016 Downtown Dubai fire [2], the 2017 fire in a 10-story hotel building in Russia [3], the 2017 Grenfell Tower fire in London [4] and the 2019 Melbourne Lacrosse tower fire, further underscore the severity of fire due to the use of combustible cladding materials.

It is imperative that non-combustible material is used in the cladding panels to build resilient and durable structures. This has also been a very clear requirement in the government guidelines. Once such example is the recent Environmental Planning

and Assessment Amendment (Identification of Buildings with Combustible Cladding) Regulation 2018, New South Wales, Australia [5], which requires building owners to identify combustible cladding on residential apartment buildings so that the councils can conduct risk assessments of the fire safety characteristics of such structures. Additionally, using specific aluminium composite panels on the exteriors of specified building types has now been completely prohibited [6]. This emphasizes the need to develop an alternate and durable material for utilizing in structures for both structural and non-structural application such as cladding.

Magnesium oxychloride cement (MOC) has been found to be a prominent choice for cladding material due to its inherent favourable characteristics. Also known as Sorel's cement, MOC is a type of non-hydraulic cement developed using light burnt magnesia (MgO) and magnesium chloride solution [7]. This cement not only promotes sustainability due to its lower energy emission in the manufacturing process, but also surpasses ordinary Portland cement (OPC) in various properties such as high early strength, low thermal conductivity, light weight, and good abrasion resistance [8]. MOC derives its strength from two main hydration phases, namely Phase 3 ($3Mg[OH]_2 \cdot MgCl_2 \cdot 8H_2O$) and Phase 5 ($5Mg[OH]_2 \cdot MgCl_2 \cdot 8H_2O$), which are stable at room temperature and contribute to rapid strength development [9,10]. However, despite its numerous benefits, the application of MOC has been limited to mostly indoor applications due to MOC's poor water resistance and brittleness.

Extensive research has been dedicated in recent years to develop water-resistant MOC [11–20]. Various additives, such as silica fume [13], fly ash (FA) [14,15], sulphates [16], aluminate [17], and phosphoric acid [18] or soluble phosphates [19] have been successfully integrated into MOC formulation to achieve hydration products that are stable in water and result in a denser and durable matrix. Recently, Guo et al. [21] incorporated the hybrid FA and silica fume with other organic additives in MOC and achieved a substantial improvement in water resistance. Their optimal mix design with 30% FA along with 0.5% sodium monofluorophosphate (MFP) and 0.5% phosphoric acid (PA) showed a compressive strength retention of more than 100% after 28 days of water immersion.

Researchers have also attempted to address the brittleness issue associated with MOC; however, there is very limited research on this matter so far. Addition of fibres to the matrix has been widely preferred in OPC-based cementitious composites as a solution for brittleness to achieve enhanced tensile performance and substantially improved tensile strain capability and flexural performance [22,23]. However, the common industrial practice for MOC has been the addition of multiple layers of grid or fibre mesh to increase the flexural strength of MOC boards [24]. This approach inevitably leads to a reduction in overall working efficiency. An alternative method of addressing brittleness through the addition of fibres to MOC has recently been assessed by various researchers. Wang et al. [25] investigated the impact of polyethylene (PE) fibre on the performance of MOC composites. Their findings revealed that PE fibre significantly improved the tensile performance of MOC composites. They reported that fibre reinforced MOC (FRMOC) exhibited a tensile strength exceeding 7 MPa and an enhanced tensile strain capability of up to 8%. Similarly, Yu et al. [24] explored the influence of ultra-high-molecular-weight PE fibre on the behaviour of MOC composites, achieving FRMOC with high strength and ductility of up to 8%. They suggested that FRMOC holds potential for practical engineering applications due to its improved strength, ductility, and satisfactory water resistance. These findings underscore the compatibility of fibres with MOC and its potential to achieve high mechanical performance.

Given the growing interest in research related to the development of MOC for both structural and non-structural applications and increase in possibility of its external use with the recent development of water-resistant MOC, it is crucial to conduct a detailed analysis of the fire resistance of MOC and fibre reinforced MOC-based cementitious composites. However, research in this specific area is scarce. Recently, Chang et al. [26] evaluated the fire performance of pure MOC mix and found a significant deterioration in both compressive

and flexural strength as the temperature increased from 100 to 500 °C. While this indicates poor performance, there is still insufficient evidence to conclusively affirm the suitability of MOC for fire-resistant applications, especially the recently formulated water-resistant MOC matrix which incorporates other additives such as FA and phosphates. This MOC matrix possesses more hydration phases than just Phase 5 and Phase 3 and hence, there is uncertainty about the role of additional binders in fire resistance. According to the authors' investigation, hitherto, no studies on fibre reinforced MOC-based cementitious composites at elevated temperatures have been reported, although fibres have demonstrated substantial role in fire resistance from the vast research conducted on fibre reinforced OPC-based cementitious composites. Low-melting point fibres such as polypropylene (PP), PE, and polyvinyl alcohol have been identified to enhance resistance against spalling. These fibres undergo melting after thermal exposure, creating channels that facilitate the dissipation of water vapours and enhance resistance against spalling [27]. Additionally, high-melting point fibres such as steel or basalt fibres have also demonstrated the ability to preserve the integrity of specimens following exposure to elevated temperatures [28].

This paper aims to analyse the behaviour of fibre reinforced MOC-based cementitious composites at both room and elevated temperatures. Hybrid combination of basalt fibres (high-melting point fibre) and PP fibres (low-melting point fibre) is utilised to improve the spalling resistance and post-exposure strength [29]. Basalt fibres are chosen not only due to their high melting point, but also due to their inert, green, and sustainable nature. The binder system is kept similar to the one proposed by Guo et al. [21], showing higher water resistance, and the fibre content is varied to study the effect of fibre on mechanical performance at elevated temperatures. The tensile and compressive tests are conducted on specimens exposed from 200 to 600 °C and 200 to 800 °C, respectively, to determine the residual tensile and compressive strength of materials. In addition, microstructural techniques such as scanning electron microscopy (SEM) and X-ray diffraction (XRD) are further utilised to analyse the decomposition stages of the matrix and fibres with temperature rise. This research, therefore, is expected to bridge existing research gaps in the fire performance of MOC, facilitating its potential extension to a broader range of industrial applications.

2. Experimental Program

2.1. Materials

To develop the fibre reinforced MOC-based cementitious composite (FRMOCC), powdered binder material consisting of MgO powder (95% purity) and FA, a $MgCl_2$ solution, fine dried sand, high-range water reducer (HRWR), water, basalt, and PP fibres were used. MgO powder was supplied by QMag Queensland, Australia and fly ash was purchased from Cement Australia. Magnesium chloride solution was prepared using magnesium chloride hexahydrate flakes (99% purity) which were purchased from Weifang Haizhiyuan Chemistry and Industry, Shouguang City, China. The $MgCl_2$ solution was prepared 24 h before casting by mixing $MgCl_2 \cdot 6H_2O$ flakes in water to achieve the required concentration.

Fine Sydney sand passing through a 355-micron sieve was used as a fine aggregate to develop the composite. The sand was oven-dried at 105 °C for 24 h and sieved before use. MFP (95%) and PA (85%) were used as additives to improve the water resistance of the mix as recommended by Guo et al. [21]. MFP was used in the form of a saturated solution with a concentration of 20%. In addition, ADVA LS780 supplied by GCP Applied technologies, Australia was utilized as HRWR to maintain flowability of the mix and to ensure homogenous fibre distribution. A combination of hybrid fibres containing basalt and PP fibre was used at various proportions to improve elevated temperature performance, and their properties are shown in Table 1. Both fibres were purchased from Guangxi Grecho Industry Co., Ltd., Nanning, Guangxi, China.

Table 1. General properties of the fibres used in the study.

Fibre Type	Length (mm)	Diameter (μm)	Tensile Strength (MPa)	Elastic Modulus (GPa)	Density (g/cm^3)	Melting Point (°C)
PP	12	23	585	5.1	0.91	165
Basalt	12	13	3300–4840	91–110	2.65	269–700 (operating temperature)

2.2. Mix Design

The basic matrix constituents and their proportions used in this study were employed based on the work by Guo et al. [21]. Their optimal mix design contained 0.5% MFP, 0.5% PA, $MgO/MgCl_2$ (M) = 9, and $H_2O/MgCl_2$ (H) = 13, where M and H are molar ratio. It should be noted that the chemical reactivity of the MgO used in their study was 49%. However, the MgO in the present study was found to have a very high reactivity of 73% evaluated as per the method described in WB/T 1019–2002 [30]. This led to an increase in the water demand and made mixing difficult. Therefore, the molar ratio of $MgO/MgCl_2$ was adjusted to 8 to account for the extreme reduction in workability. It was found that with M8-H13, the mix attained sufficient flowability to be homogenously mixed. The sand to binder ratio was 0.23 as recommended by Yu et al. [24]. The details of the mix constituents and their relative proportion are shown in Table 2. Three mixes were selected to study the effect of fibre addition on the room temperature and elevated temperature properties of FRMOCC. The total fibre volume content was maintained at 2.0%, which is the typical fibre content for fibre reinforced cementitious composites. One mix contained only 2% basalt fibres as also adopted by Xu et al. [31], while in the other two mixes, the total volume contained both PP and basalt fibres. PP fibre dosage was varied from 0.3 to 0.5%, aligning with previous recommendations [28,32] for potentially best spalling resistance. A general outline of the experimental plan is further illustrated in Figure 1. The mix ID is defined by MXBFYPP where M means the base matrix, which is same for all the three mixes, XBF denotes X% basalt fibre and YPP denotes Y% PP fibre.

Table 2. Mix designs considered in the present study.

Mix ID	Molar Ratio of All Mixes		Sand/Binder	FA	PA	MFP	Basalt	PP
	$MgO/MgCl_2$	$H_2O/MgCl_2$						
M2.0BF0PP	8	13	0.23	30%	0.5%	0.5%	2.0%	-
M1.7BF0.3PP	8	13	0.23	30%	0.5%	0.5%	1.7%	0.3%
M1.5BF0.5PP	8	13	0.23	30%	0.5%	0.5%	1.5%	0.5%

2.3. Mixing Procedure and Sample Preparation

The mixing initiated with dry blending of the binder material, namely MgO powder, FA, and sand for about 2 min. Separately, the concentrated $MgCl_2$ solution was mixed with MFP and PA using a magnetic stirrer for 1–2 min to achieve uniform dispersion. Thereafter, the solution was added to the dry mix and the mixing continued for another 2–3 min. Depending on the consistency of the mix at this stage, an appropriate dose of HRWR was added to achieve a flowable mix. After the mix was sufficiently flowable, fibres were slowly added, and the mixing continued for another 3 min at low speed and the last 2 min at high speed. After mixing, the resultant mix was poured into the greased cube and dog-bone moulds. Cubic specimens of 50 mm size were cast for compressive strength test, whereas dog bone specimens of size 340 mm (length) × 50 mm (width) × 13 mm (thickness) were used for tensile strength test. Three specimens were prepared for each set to obtain representative test results. These moulds were properly compacted using the vibration table to avoid entrapment of air voids. Flow table and setting time test were also carried out alongside using the freshly prepared mix. The moulds were wrapped in a polythene sheet after casting, and the samples were demoulded after 24 h. The samples were then

kept for curing under controlled conditions (20 ± 2 °C and 65 ± 5% relative humidity) for 28 days.

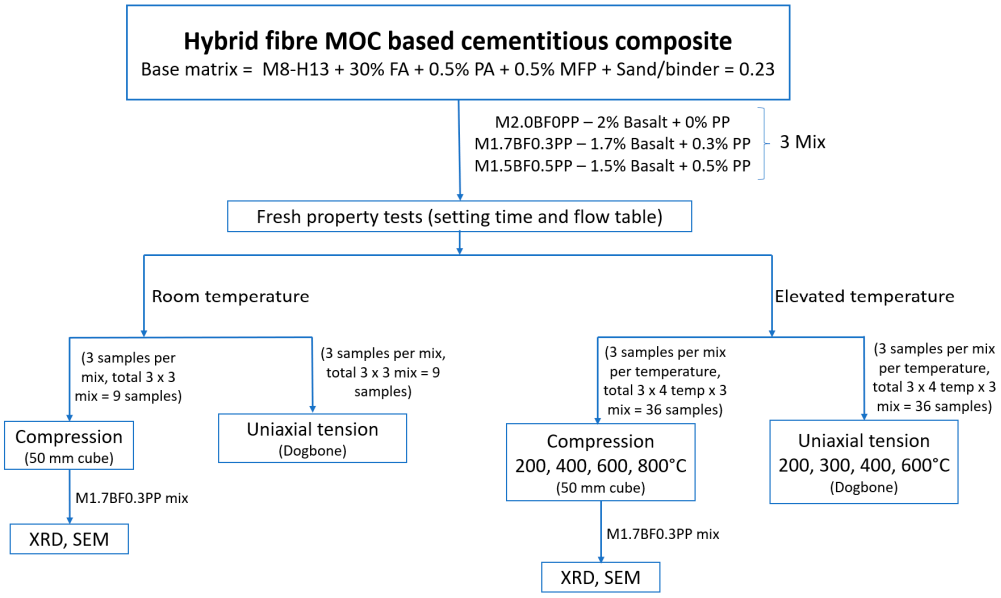

Figure 1. Outline of the experimental plan.

2.4. Testing Procedures

2.4.1. Flowability, Setting Time and Hardened Density

The flowability of a fresh FRMOCC mix was measured using the flow table as per ASTM C1437 [33]. Similarly, the initial and final setting time of the different FRMOCC mixes were assessed using the Vicat apparatus as per the procedure stated in ASTM C191 [34]. The hardened density of FRMOCC specimens was assessed after measuring the size and mass of the specimens.

2.4.2. Compressive and Tensile Tests

Cube specimens, 50 mm in size, were tested at a loading rate of 20 MPa/min using the Instron universal testing machine (Figure 2a) to obtain compressive strength. Dog-bone specimens with a cross-sectional area of 30 mm × 13 mm in the reduced section and a gauge length of 60 mm were used for the uniaxial tension test. The tests were conducted at displacement-controlled loading rate of 0.1 mm/min using the Instron tensile testing machine with a 250 kN capacity. Two external linear variable displacement transducers (LVDTs) were attached on either side of the specimen via a steel rig to measure the displacement as shown in Figure 2b. Three samples were tested for each set and each temperature range to obtain a representative result.

2.4.3. Elevated Temperature Testing

The specimens allocated for elevated temperature testing were initially weighed and placed inside a vertical split tube furnace as shown in Figure 3. For cubic specimens, the exposure temperature was selected as 200, 400, 600, 800 °C, whereas the peak exposure temperature for dog-bone specimens was 200, 300, 400, and 600 °C. All specimens were heated at a rate of 2 °C/min and the temperature was maintained for another 2 h at each respective peak temperature. These heating parameters were found suitable for isothermal heating in previous literature [28]. Following heating, the samples were allowed cooling naturally inside the muffle furnace for 24 h, and the specimens were re-weighed to estimate mass loss. Thereafter, the specimens were tested under compression or tension to measure their residual performance.

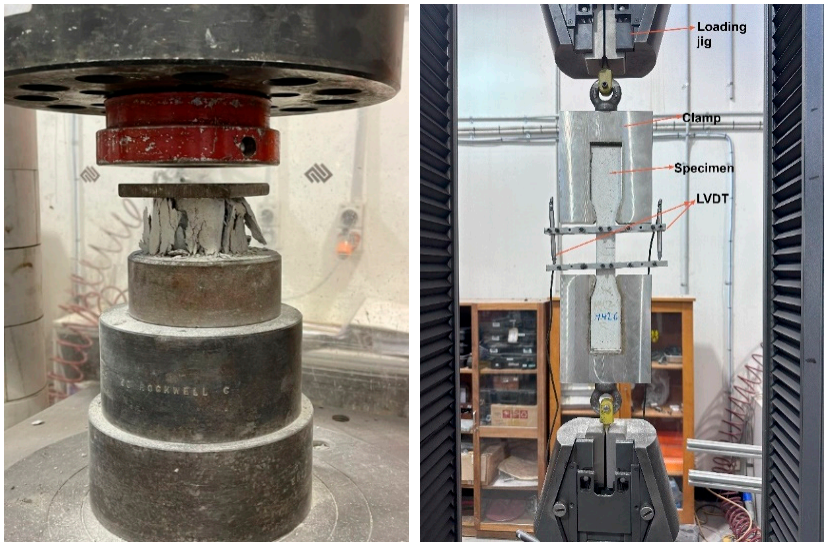

(**a**) (**b**)

Figure 2. Testing setup for mechanical properties tests. (**a**) Compression strength test. (**b**) Uniaxial tensile test.

Figure 3. Split tube furnace used in the present study.

2.4.4. Microstructural Tests

SEM and XRD analyses were utilized to investigate the morphology of the FRMOCC mix and analyse the decomposed products in order to gain a more comprehensive understanding of residual properties. Following compression testing, small specimens were extracted from the core of each set and immersed in acetone for a minimum of 48 h to halt further hydration. Subsequently, part of the sample was converted to powdered form for XRD analysis, and the remaining solid part was used for SEM analysis. For SEM, solid samples were carbon-coated and examined using the Phenom XL SEM, operating at an accelerating voltage of 15 kV and a chamber pressure of 1 Pa. XRD patterns were obtained using the Bruker D8 Advance XRD analyser at a scan range of 5 to 80° 2θ.

3. Results and Discussion

3.1. Fresh Properties

Flowability and setting time are both essential parameters to establish the usability of the material for a specific application. Both parameters are significantly affected by water content and amount of HRWR, which were kept constant. However, since the amount

of fibre differed in each mix, the flow value and setting time was found to be different. Table 3 shows the flowability and setting time values with change in fibre content. In general, the flow value of all the mixes remained in the range similar to that of engineered cementitious composites [35]. Moreover, though the setting time did not show any clear trend with change in fibre dosage, a comparison could be made with the values without fibres as reported by Guo et al. [21]. Their M9-H13 mix with 30% FA showed a flow value of approximately 190 mm and initial and final setting times of 3.6 and 4.25 h. Therefore, it can be observed that the introduction of fibres led to a decrease in flow values (152–160 mm) and an increase in both initial (5.15–5.75 h) and final (6.75–7.15 h) setting time. This decline in flowability may be attributed to internal flow resistance resulting from the fibre-matrix network, and the entanglement or clumping of basalt fibres could have further contributed to this reduction. Conversely, the prolonged setting time can be explained by the retardation in hydration due to the presence of an additional fibre–matrix interface. In contrast, mixtures without fibres lack this interface, resulting in quicker setting times.

Table 3. Flow table and setting time test results for different mixes.

	M2.0BF0PP	**M1.7BF0.3PP**	**M1.5BF0.5PP**
Flow value (mm)	158	160	152
Initial setting time (hours)	5.5	5.15	5.75
Final setting time (hours)	6.75	7	7.15

3.2. Hardened Density

Density was determined by calculating the ratio of the dry weight of 50 mm cube specimens (measured at the end of the curing period) to their respective volume. The resulting density ranged from 1810 to 1928 kg/m^3 as shown in Table 4, which was significantly lower than that of conventional concrete or fibre reinforced cementitious composites, showing the merits of lighter weight FRMOCC than conventional ordinary Portland cement. Moreover, the density of mix M2.0BF0PP with no PP fibre was found to be higher than that of other two mixes with PP fibres. This indicates that increasing the PP fibre content leads to reduction in density. This outcome was anticipated due to the inherently lower density of PP fibres, and it may also have been influenced by the mixing process of the fibres.

Table 4. Hardened density for different mixes.

	M2.0BF0PP	**M1.7BF0.3PP**	**M1.5BF0.5PP**
Density (kg/m^3)	1920 $\pm$ 8.83	1902 $\pm$ 4.81	1813 $\pm$ 3.41

Variation in density can be further explained by setting time observations. It can be observed that the mix containing 0.5% PP fibre exhibited the longest setting time, which could be attributed to the presence of a greater fibre–matrix interface, prolonging the setting time. This observation suggests the potential presence of fibre entanglement, with compaction possibly playing a crucial role in determining density. Nonetheless, FRMOCC demonstrated lower density compared to engineered cementitious composites which have a density of around 2100 kg/m^3 [36]. This supports its potential for applications where reduced handling efforts are desirable.

3.3. Mechanical Properties

3.3.1. Mechanical Performance of FRMOCC at Ambient (Room) Temperature

Figure 4 shows compressive and tensile strength variation of the material with the changes in fibre content at ambient temperature. Both strength types exhibited a similar pattern, with the mix containing only basalt fibres (M2.0BF0PP) demonstrating the highest strength.

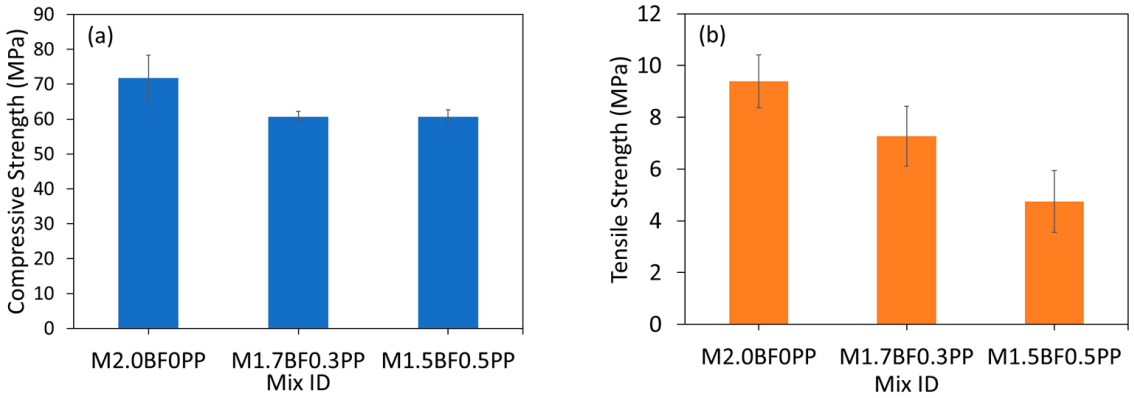

Figure 4. (**a**) Compressive and (**b**) tensile strength of different mixes at room temperature.

For compressive strength (Figure 4a), the results demonstrate that the strength of the mix with 2% basalt fibres was the highest and it decreased with the addition of PP fibre. Compressive strength reached a plateau at 0.3% PP fibre content, beyond which there was no significant change. M2.0BF0PP exhibited compressive strength approximately 15.4% higher than that of M1.7BF0.3PP and M1.5BF0.5PP, indicating a positive influence of basalt fibres on compressive strength. Moreover, despite the addition of PP fibres, the strength of FRMOCC did not significantly decrease as claimed in some studies [37] and still met high-strength criteria, demonstrating the effectiveness of fibre hybridization.

Tensile strength (Figure 4b) was also highest in the sample with 2% basalt fibres, but it continuously decreased with an increase in fibre content. PP fibres, being low modulus, did not contribute significantly to tensile strength. In contrast, high-modulus basalt fibres typically contribute to tensile strength, resulting in higher strength when their content is higher. Consequently, the tensile strength of the mix with 2% basalt fibres (M2.0BF0PP) was 22.6% and 49.4% higher than that of M1.7BF0.3PP and M1.5BF0.5PP, respectively.

3.3.2. Mechanical Performance of FRMOCC at Elevated Temperatures

Compressive Strength

Figure 5a shows the variation in normalized compressive strength of FRMOCC with the change in fibre content at different temperatures. The normalized compressive strength is defined as the ratio of the average compressive strength of the specimen at a specific temperature to the average compressive strength of specimen at room temperature. It can be observed that compressive strength consistently decreases as temperature increases, with a steep drop between 200 and 600 °C. The results demonstrated that M1.5BF0.5PP outperformed M2.0BF0PP and M1.7BF0.3PP. At 200 °C, M2.0BF0PP retained a ratio of 0.73 with compressive strength of 52.63 MPa, while M1.7BF0.3PP and M1.5BF0.5PP showed a slight increase in compressive strength with ratios of 1.02 (61.09 MPa) and 1.03 (62.44 MPa), respectively. The strength consistently decreased after this temperature for all the mixes. At 400 °C, the strength retained by mix M2.0BF0PP was approximately 30%, whereas the same for mix M1.5BF0.5PP was observed to be 88%. The difference between mixes with and without PP fibres subsided after 400 °C and at 800 °C; the compressive strength of all the specimens became almost negligible, ranging between 1 and 2 MPa. For all temperature ranges, a higher residual compressive strength was observed for mix M1.5BF0.5PP. This was particularly clear above 400 °C and may have been due to the higher amount of PP fibres. The presence of PP fibres in M1.7BF0.3PP and M1.5BF0.5PP may have facilitated the formation of channels within the matrix, aiding in the dissipation of pore pressure and reducing thermal stresses, thus resulting in higher strength. This also shows that basalt fibres did not play any significant role in retaining compressive strength.

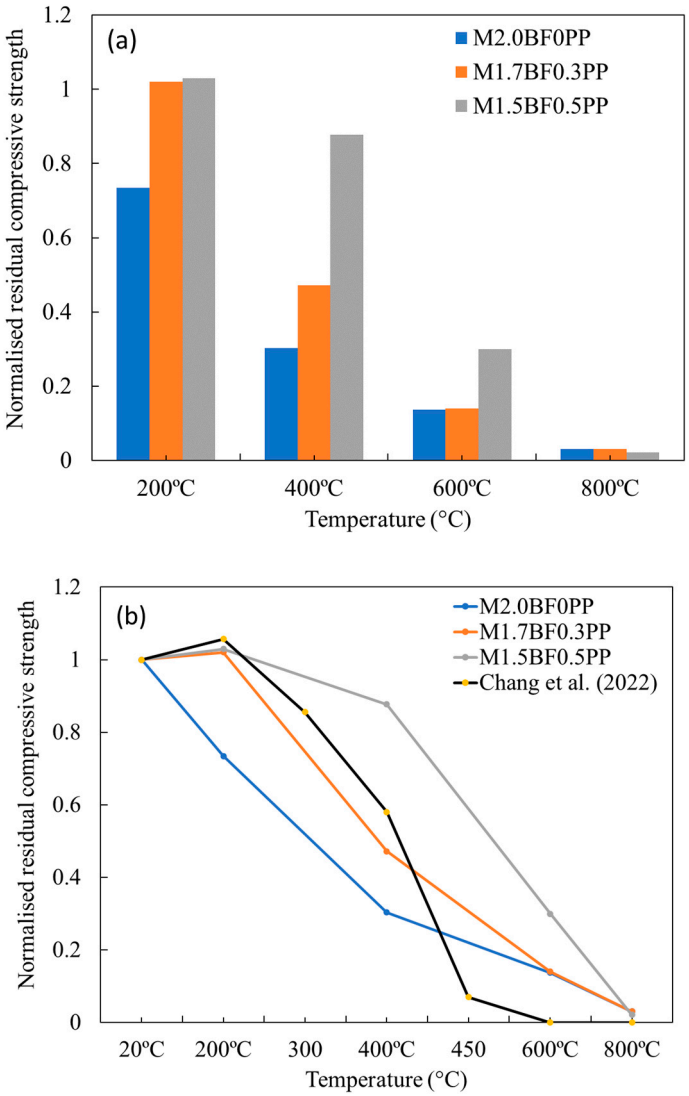

Figure 5. Normalised residual compressive strength at elevated temperatures (**a**) comparison of three mixes (**b**) comparison of results with existing literature [26].

A comparison with a recent study by Chang et al. [26] in Figure 5b further highlights the effectiveness of the addition of fibres in enhancing elevated temperature resistance. Mix M1.5BF0.5PP exhibited substantially higher residual compressive strength especially beyond 200 °C compared to the reported results, emphasizing the effectiveness of PP fibres in retaining higher residual strength. In fact, residual strength after 400 °C in all mixes surpassed that of the mix without fibres analysed by Chang et al. [26]. This further confirmed the crucial role of fibres in retaining high residual strength, especially at very high temperatures.

Tensile Strength

Figure 6 shows the normalization residual tensile strength of different mixes at elevated temperatures. Normalized tensile strength is defined as the ratio of the average peak tensile stress of the specimen at a specific temperature to the average peak tensile stress of specimen at room temperature. It can be observed that as the temperature increased from 20 to 200 °C, there was drastic reduction in tensile strength. The strength reduced by approximately 71–85% at 200 °C with the 2% basalt fibre mix showing the least reduction. This clearly showed the role of matrix and fibres in providing tensile strength. Since mix M2.0BF0PP only contained basalt fibres, a sudden reduction at 200 °C might have been due to the

onset of decomposition of hydration products and evaporation of water. Moreover, the other two mixes also contained PP fibre and their melting likely contributed to a more pronounced reduction in tensile strength.

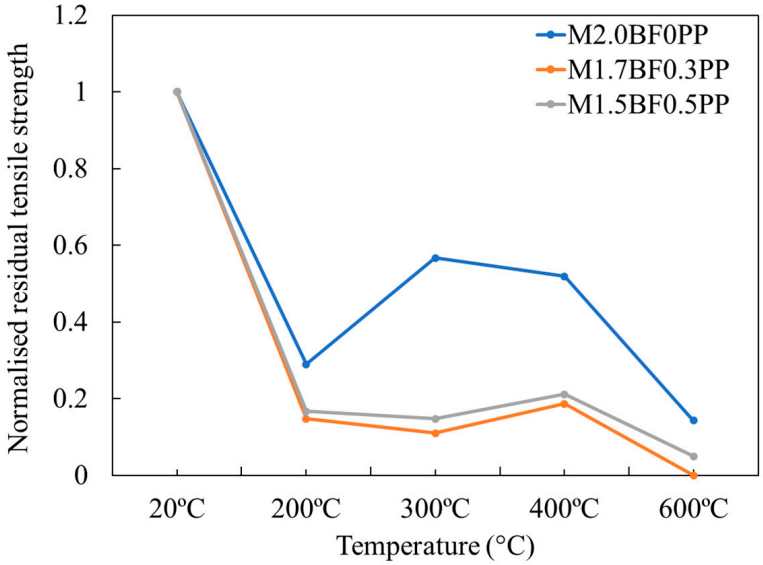

Figure 6. Normalised residual tensile strength of different mixes at elevated temperatures.

On further increase in temperature, the strength slightly increased for the mix with 2% basalt fibre. This may have been due to the release of pore pressure and improvement of bond between matrix and basalt fibre. This trend continued till 400 °C, showing that the onset of decomposition did not affect tensile strength significantly from 200 to 400 °C and the remaining basalt fibres continued to provide some resistance to tensile stresses. However, with increase in temperature beyond 400 °C, decomposition was almost complete for the main hydration phases, and therefore, tensile strength at 600 °C was only negligible.

Tensile Stress–Strain Behaviour

Figure 7 presents the graph highlighting the typical tensile stress–strain relationship for the three mixes at temperature ranging from 20 °C (control) to 400 °C. It should be noted that though the specimens were tested at 600 °C, it was not possible to obtain the stress–strain relationship considering that the specimens had very low thickness and the matrix underwent serious degradation. It can be observed from Figure 7 that the stress–strain curve for the mix with 2% basalt fibres showed an initial rise with a peak around 7.74 MPa at 0.03% strain. Mix M1.7BF0.3PP with 1.7% basalt and 0.3% PP fibre also showed similar behaviour, with peak tensile stress reaching 7.0 MPa at strain of 0.05%. On further increase in the PP fibre content as for Mix M1.5BF0.5PP, the peak tensile stress decreased with the peak strain remaining at the same range. For all the mixes, the stress–strain curve followed a consistent trend of initial ascent and then a sudden drop post peak.

On increasing the temperature to 200 °C, there was a drastic change in tensile stress–strain behaviour. The peak stress decreased considerably, and the curve exhibited a flatter tendency, indicating a higher value of peak strain. This value showed marginal improvement at an exposed temperature of 400 °C. The slightly improved behaviour may be attributed to lesser internal stress resulting from vapor pressure. Up to 200 °C, significant water evaporation and fibre melting occur, initially limiting space for water vaporisation and leading to internal stresses. However, as the temperature increases further, the situation improves since PP fibres completely melt, allowing better vapor migration and preventing internal stress and associated cracks [27,38].

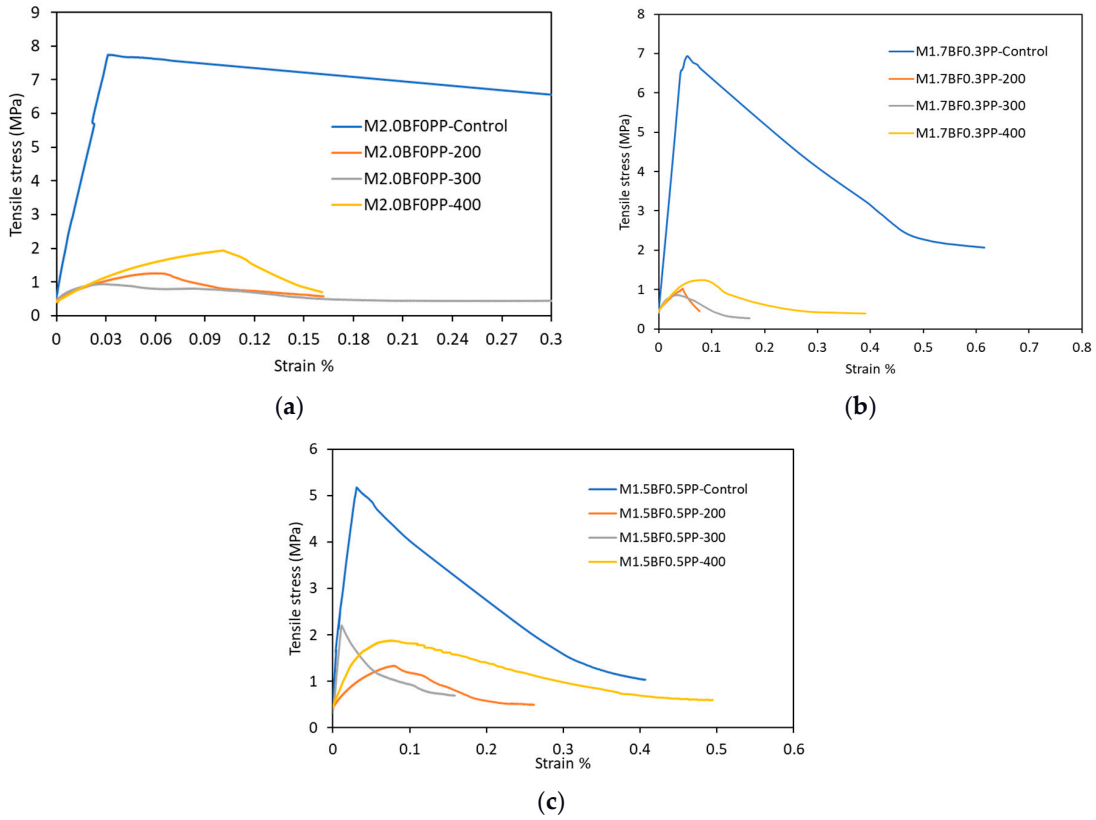

Figure 7. Typical tensile stress–strain behaviour of different mixes at elevated temperatures. (**a**) M2.0BF0PP. (**b**) M1.7BF0.3PP. (**c**) M1.5BF0.5PP.

3.4. Qualitative and Microstructural Characterisation

3.4.1. Surface Appearance

A preliminary assessment of the fire performance could be estimated from the surface change occurring during thermal exposure. Figure 8 shows the surface appearance of M1.7BF0.3PP mix specimens at different temperatures. The specimens appeared grey at room temperature, transitioning to a lighter shade at 600 °C and eventually turning white at 800 °C. At 800 °C, the matrix underwent significant decomposition, and the white colour may be attributed to residual MgO, a byproduct at that temperature. It is important to note that despite the difference in fibre content, different mix specimens did not show any apparent differences in crack pattern, confirming the effectiveness of basalt-PP hybridisation as also highlighted in previous studies [29]. Minor cracks were only visible in the specimen at 800 °C and all the specimens remained intact without any spalling. The resistance of spalling and cracking is generally found to increase with the addition of PP fibres. However, in this particular case, the lower heating rate and the small specimen size might not be enough to lead to high buildup pressure which could have prevented the occurrence of spalling.

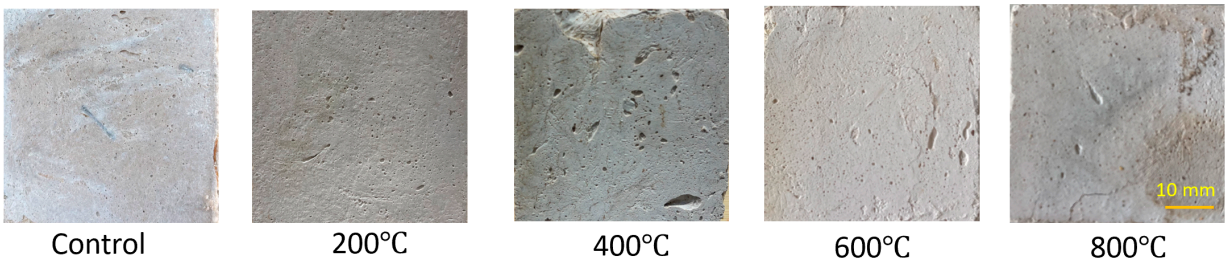

Figure 8. Surface appearance of FRMOCC specimens at elevated temperatures.

3.4.2. Mass Loss

Figure 9 shows the mass loss occurring in different dog-bone specimens when exposed to temperatures from 200 to 600 °C. It can be observed that mass loss of all the mixes was fairly similar, suggesting that the PP fibre did not significantly contribute to mass loss. Mass loss increased to approximately 8% at 200 °C and consistently increased with increase in temperature reaching more than 31% at 600 °C. This is in contrast to normal concrete or engineered cementitious composites, where mass loss predominantly occurs during the initial temperature rise and increases at a relatively modest rate after 400 °C, reaching levels of 17–20% [28,39].

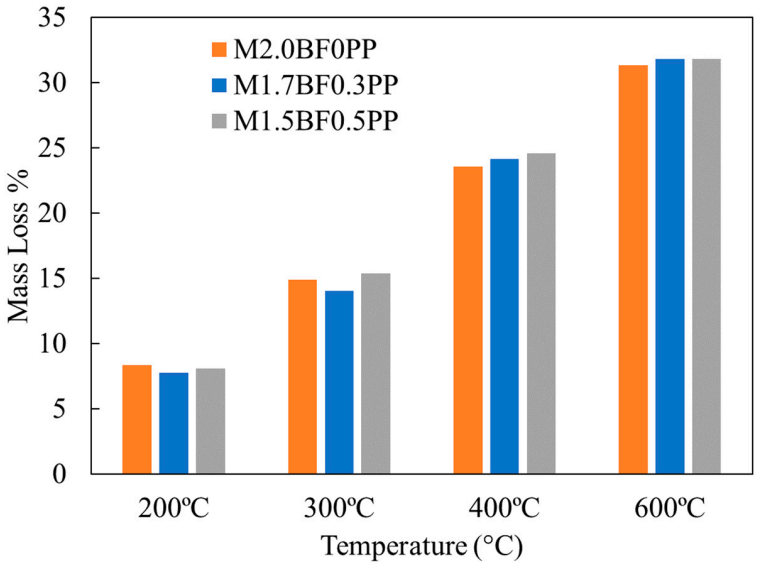

Figure 9. Mass loss in dog-bone specimens of different mixes at elevated temperatures.

Typically, the primary factor contributing to mass loss is the evaporation of free, absorbed, or chemically bound water, and this is closely linked to the decomposition of hydration products. However, FRMOCC differs substantially in terms of hydration compounds from normal concrete or cementitious composites, leading to distinct patterns of mass loss. Due to the presence of various temperature-sensitive hydration phases in the hydration products of MOC, mass loss is also influenced by these phases. The thermal decomposition of the primary hydration phases of MOC, specifically Phase 5 and Phase 3, occurs at different stages as shown below through Equations (1)–(7) [21]. It can be clearly seen that both Phase 5 and Phase 3 start decomposing as early as 100 °C and their decomposition is almost complete until 500 °C. This might be the reason of a consistent increase in mass loss with increase in temperature. Moreover, the decomposition of carbonate phase also starts beyond 500 °C (Equation (8)), which might have further contributed to the loss in mass.

$$5Mg(OH)_2 \cdot MgCl_2 \cdot 8H_2O \rightarrow 5Mg(OH)_2 \cdot MgCl_2 \cdot 4H_2O + 4H_2O\ (40\ ^\circ C – 110\ ^\circ C), \quad (1)$$

$$5Mg(OH)_2 \cdot MgCl_2 \cdot 4H_2O \rightarrow 5Mg(OH)_2 \cdot MgCl_2 + 4H_2O\ (100\ ^\circ C – 230\ ^\circ C), \quad (2)$$

$$5Mg(OH)_2 \cdot MgCl_2 \rightarrow MgCl_2 \cdot H_2O + 4H_2O + 5MgO\ (350\ ^\circ C – 500\ ^\circ C), \quad (3)$$

$$3Mg(OH)_2 \cdot MgCl_2 \cdot 8H_2O \rightarrow 3Mg(OH)_2 \cdot MgCl_2 \cdot 4H_2O + 4H_2O\ (40\ ^\circ C – 125\ ^\circ C), \quad (4)$$

$$3Mg(OH)_2 \cdot MgCl_2 \cdot 4H_2O \rightarrow 3Mg(OH)_2 \cdot MgCl_2 + 4H_2O\ (125\ ^\circ C – 215\ ^\circ C), \quad (5)$$

$$3Mg(OH)_2 \cdot MgCl_2 \rightarrow MgCl_2 \cdot H_2O + 4H_2O + 3MgO\ (350\ ^\circ C – 500\ ^\circ C), \quad (6)$$

$$MgCl_2 \cdot H_2O \rightarrow MgO + 2HCl\ (350\ ^\circ C – 500\ ^\circ C), \quad (7)$$

$$MgCO_3 \rightarrow MgO + CO_2\ (500\ ^\circ C – 900\ ^\circ C). \quad (8)$$

3.4.3. Microstructural Characteristics

Microstructural characterisation provides additional insights into the behaviour of FRMOCC. Figure 10 shows the XRD graphs of the M1.7BF0.3PP mix at different temperature range. Since the base matrix of all mixes is similar, the microstructure (obtained through XRD and SEM analysis) is compared for only one mix at different temperatures to offer a preliminary understanding of phase changes. As can be seen from Figure 10, Phase 5 could be seen having a prominent peak in the control samples at around 12° and 21.5° 2θ. The intensity of this phase decreases on increase in temperature with the phase completely disappearing after 400 °C. This could be closely linked to the generation of MgO. Notably, MgO peaks are absent in the control sample, but their intensity increases with temperature, with a distinct peak emerging beyond 400 °C. The peaks of MgO at 43° and 62.4° 2θ are very distinct after this temperature, confirming the decomposition of hydration phases, and at 800 °C, primarily the peak of MgO remains. It should further be noted that due to the decomposition of Phase 5 and other hydration compounds, peaks of Magnesium hydroxide are also visible at 18.5°, 37.7, 50.9° 2θ, especially after 200 °C, but gradually subside as this compound also decomposes to MgO.

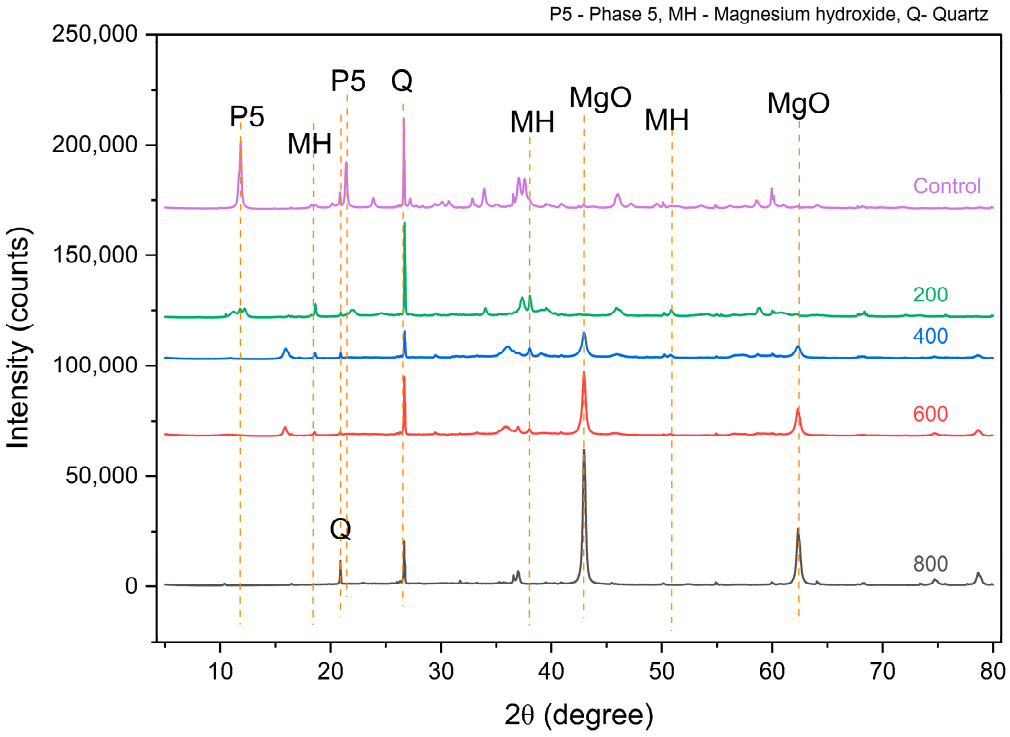

Figure 10. XRD graphs of the M1.7BF0.3PP mix at different temperature exposure.

The findings could further be substantiated by the observations from scanning electron microscope (Figures 11 and 12). As depicted in Figure 11, both types of fibres exhibited strong bonding with the matrix which might have resulted in better compressive and tensile performance. The fibres were identified in the micrographs using their diameter measurements. Moreover, the interface between the aggregate and hydration products looks very confined as shown in Figure 12a. Figure 12b further shows the micrograph at 200 °C which clearly displays the intact basalt fibres and some channels due to the melting of PP fibres. As previously mentioned, the melting of PP fibres led to these vacant channels which in turn helped in the dissipation of pore pressure and may have reduced internal stresses [27]. Figure 12c shows the decomposed FRMOCC, showing MgO in a light colour. This indicates that FRMOCC decomposed to MgO and may explain the inferior performance at this temperature.

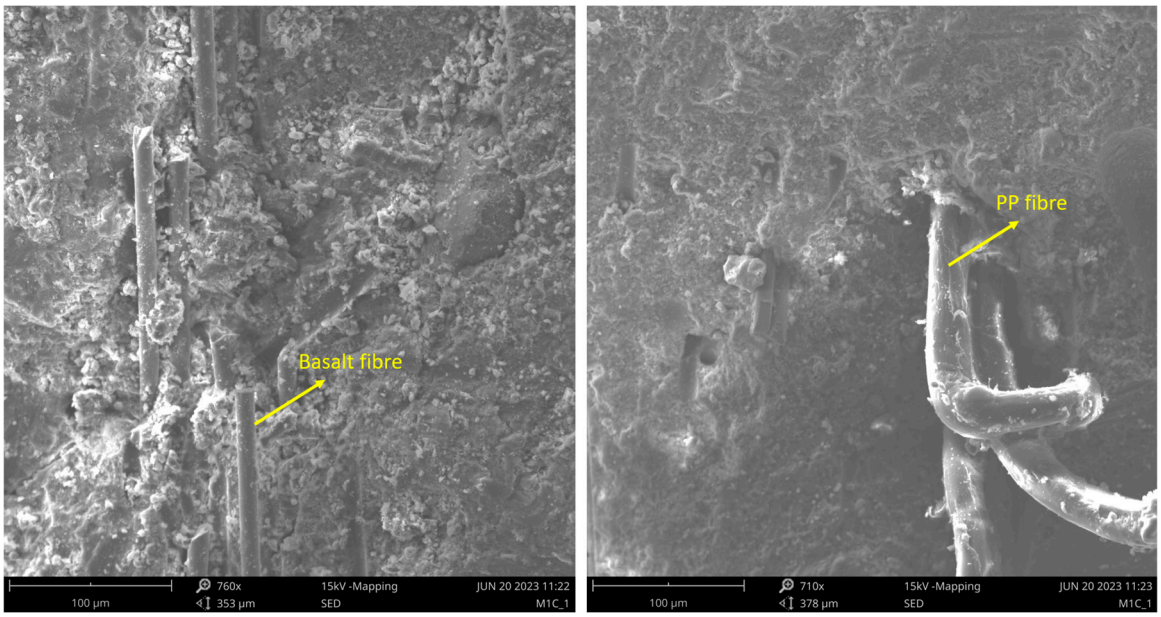

Figure 11. SEM micrographs of M1.7BF0.3PP specimens at room temperature.

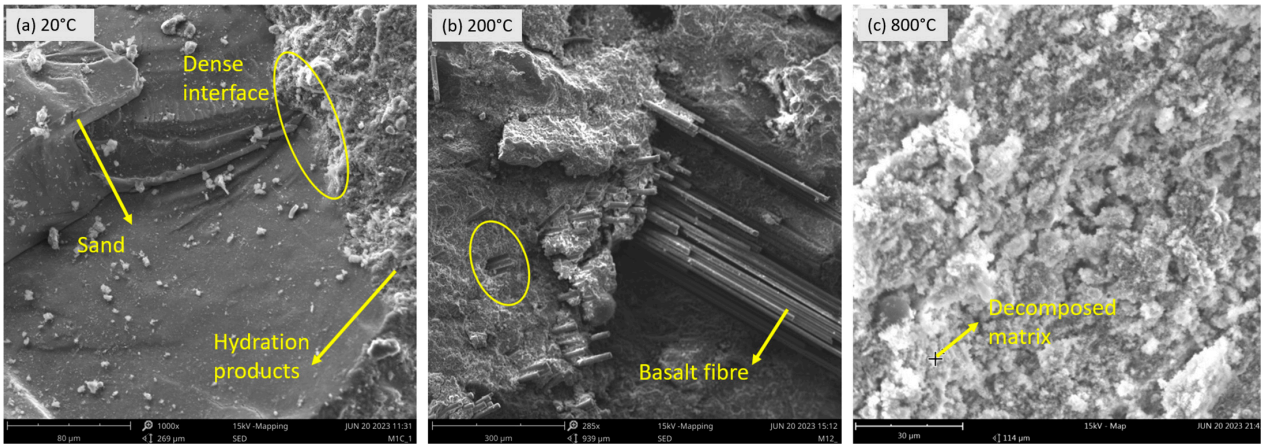

Figure 12. SEM micrographs of M1.7BF0.3PP specimens at (**a**) 20 °C (**left**); (**b**) 200 °C (**middle**); (**c**) 800 °C (**right**).

Overall, the XRD and SEM observations and the highlighted decomposition compounds validate the significant increase in mass loss and the reduction in compressive and tensile strength with increase in temperature. This underscores that the hydration phases of FRMOCC are not stable when exposed to elevated temperatures. Consequently, there is a need for further research to investigate the viability of alternative binder materials in the MOC matrix that could offer stability and enhance overall performance at a high-temperature range.

4. Conclusions

This study advances the knowledge crucial for the implementation of FRMOC-based cementitious composites at a structural scale by analysing the performance at room and elevated temperatures. Three different types of mixes with varying content of basalt and PP fibres are adopted and their residual compressive and tensile strength as well as microstructural evolution are analysed at different temperature ranges. Based on the observations, the following conclusions can be drawn:

- The addition of fibres adversely affected flowability and setting time, resulting in decreased flowability and increased setting time. However, the flow value remained within a similar range (150–160 mm) as OPC-based cementitious composites.
- Mix M2.0BF0PP exhibited the highest compressive strength (71.71 MPa) and tensile strength (9.39 MPa) at room temperature, indicating that basalt fibres contribute positively to strength. However, the strength relatively reduced with increase in PP fibre content.
- All FRMOCC specimens suffered significant mass loss with increase in temperature, with mass loss exceeding 31% at 600 °C. This was found to be substantially higher than mass loss observed in OPC-based cementitious composites and was due to the continuous decomposition of main hydration phases which was further confirmed through XRD and SEM analysis.
- Compressive strength significantly decreased with increase in temperatures, especially at 800 °C, where it reduced by over 95%. Specimen with the highest volume of PP fibre (M1.5BF0.5PP) demonstrated the best overall performance, potentially due to the melting effect of PP fibres, which aided in vapor pressure release and reduced internal stresses. Furthermore, the performance of this mix was found to be substantially better than the previously reported residual strength of MOC without fibres, providing additional confirmation of the beneficial effect of fibre addition in improving fire performance.
- Tensile strength also suffered significant loss with an increase in temperature. A decrease of 71–85% was observed at 200 °C. Contrary to compressive strength, the specimens with PP fibre suffered a higher decrease as a result of their melting. Mix M2.0BF0PP showed the best performance in terms of tensile strength followed by mixes M1.5BF0.5PP and M1.7BF0.3PP.
- No significant cracks or spalling were observed in any of the specimens exposed to temperatures ranging from 200 to 800 °C. This might be due to the adopted low heating rate and positive influence of fibres.
- Considering the substantial performance loss in FRMOCC specimens at elevated temperatures, it is recommended that future studies should be directed towards addition of binders to generate more thermally stable hydration phases. This could enhance performance, allowing for broader application in various structural elements and non-structural uses, such as cladding panels.

Author Contributions: Conceptualization, S.R. and Y.Z.; methodology, S.R.; formal analysis, P.S., P.C.E. and S.R.; investigation, P.S., P.C.E., F.A. and S.R.; resources, Y.Z.; data curation P.S., P.C.E., F.A. and S.R.; writing—original draft preparation, S.R.; writing—review and editing, P.S., P.C.E., F.A., S.R. and Y.Z.; visualization, P.S., P.C.E. and S.R.; supervision, Y.Z.; project administration, Y.Z. All authors have read and agreed to the published version of the manuscript.

Funding: This research was funded by the Australian Government through Australian Research Council Discovery Project (DP220103043). Support of School of Engineering, Design and built environment, Western Sydney University through candidature support fund is also acknowledged.

Data Availability Statement: The data used in this study has already been included in the manuscript.

Acknowledgments: The authors would like to acknowledge the Advanced Materials Characterisation Facility (AMCF) of Western Sydney University for access to its instrumentation and staff.

Conflicts of Interest: The authors declare no conflict of interest.

References

1. Soufeiani, L.; Nguyen, K.T.Q.; White, N.; Foliente, G.; Wang, H.; Aye, L. Fire safety performance of 3D GFRP nanocomposite as a cladding material. *Fire Saf. J.* **2022**, *133*, 103670. [CrossRef]
2. Nguyen, K.T.; Weerasinghe, P.; Mendis, P.; Ngo, T. Performance of modern building facades in fire: A comprehensive review. *Electron. J. Struct. Eng.* **2016**, *16*, 69–87. [CrossRef]
3. Cockburn, H. *Russia Hotel Fire: Two Dead after Blaze Engulfs 10-Storey Building in Rostov on Don*; Independent Digital News & Media: London, UK, 2017.

4. Kirkpatrick, D.D.; Hakim, D.; Glanz, J. Why Grenfell Tower Burned: Regulators Put Cost Before Safety. *New York Times*, 24 June 2017.
5. Environmental Planning and Assessment Amendment (Identification of Buildings with External Combustible Cladding) Regulation. The Environmental Planning and Assessment Act 1979. 2018. Available online: https://legislation.nsw.gov.au/view/pdf/asmade/sl-2018-499 (accessed on 14 December 2023).
6. Watermeyer, R.P.E.; Strydom, K. The fire safety performance of internal and external walls in multi-storey buildings. *Civ. Eng. Mag. S. Afr. Inst. Civ. Eng.* **2020**, *28*, 28–31.
7. Li, K.; Wang, Y.S.; Yao, N.; Zhang, A. Recent progress of magnesium oxychloride cement: Manufacture, curing, structure and performance. *Constr. Build. Mater.* **2020**, *255*, 119381. [CrossRef]
8. Huang, T.; Yuan, Q.; Deng, D. The role of phosphoric acid in improving the strength of magnesium oxychloride cement pastes with large molar ratios of $H_2O/MgCl_2$. *Cem. Concr. Compos.* **2019**, *97*, 379–386. [CrossRef]
9. Cole, W.; Demediuk, T. X-ray, thermal, and Dehydration studies on Magnesium oxychlorides. *Aust. J. Chem.* **1955**, *8*, 234–251. [CrossRef]
10. Demediuk, T.; Cole, W.; Hueber, H. Studies on magnesium and calcium oxychlorides. *Aust. J. Chem.* **1955**, *8*, 215–233. [CrossRef]
11. He, P.; Poon, C.S.; Tsang, D.C. Effect of pulverized fuel ash and CO_2 curing on the water resistance of magnesium oxychloride cement (MOC). *Cem. Concr. Res.* **2017**, *97*, 115–122. [CrossRef]
12. Guo, Y.; Zhang, Y.; Soe, K.; Hutchison, W.D.; Timmers, H.; Poblete, M.R. Effect of fly ash on mechanical properties of magnesium oxychloride cement under water attack. *Struct. Concr.* **2019**, *21*, 1181–1199. [CrossRef]
13. Yu, H.F.; Liu, P.Q.; Wang, W.H. The properties of silica fume-magnesium oxychloride cement materials. *Acta Met-Allurgica Sin. Engl. Lett.* **1999**, *12*, 1038.
14. Chau, C.; Chan, J.; Li, Z. Influences of fly ash on magnesium oxychloride mortar. *Cem. Concr. Compos.* **2009**, *31*, 250–254. [CrossRef]
15. Chan, J.; Li, Z. Influence of fly ash on the properties of magnesium oxychloride cement. In *Measuring, Monitoring and Modeling Concrete Properties: An International Symposium Dedicated to Professor Surendra P. Shah, Northwestern University, USA*; Springer: Amsterdam, The Netherlands, 2006; pp. 347–352.
16. Li, Y.; Li, Z.; Pei, H.; Yu, H. The influence of $FeSO_4$ and KH_2PO_4 on the performance of magnesium oxychloride cement. *Constr. Build. Mater.* **2016**, *102*, 233–238. [CrossRef]
17. Dehua, D.; Chuanmei, Z. The effect of aluminate minerals on the phases in magnesium oxychloride cement. *Cem. Concr. Res.* **1996**, *26*, 1203–1211. [CrossRef]
18. Chen, X.; Zhang, T.; Bi, W.; Cheeseman, C. Effect of tartaric acid and phosphoric acid on the water resistance of magnesium oxychloride (MOC) cement. *Constr. Build. Mater.* **2019**, *213*, 528–536. [CrossRef]
19. Deng, D. The mechanism for soluble phosphates to improve the water resistance of magnesium oxychloride cement. *Cem. Concr. Res.* **2003**, *33*, 1311–1317. [CrossRef]
20. Gomes, C.M.; Cheung, N.; Gomes, G.M.; Sousa, A.K.; Peruzzi, A.P. Improvement of water resistance in magnesia cements with renewable source silica. *Constr. Build. Mater.* **2020**, *272*, 121650. [CrossRef]
21. Guo, Y. *Development of Water-Resistant Magnesium Oxychloride Cement*; UNSW Sydney: Sydney, Australia, 2020.
22. di Prisco, M.; Plizzari, G.; Vandewalle, L. Fibre reinforced concrete: New design perspectives. *Mater. Struct.* **2009**, *42*, 1261–1281. [CrossRef]
23. Li, V.C. On engineered cementitious composites (ECC) a review of the material and its applications. *J. Adv. Concr. Technol.* **2003**, *1*, 215–230. [CrossRef]
24. Yu, K.; Guo, Y.; Zhang, Y.; Soe, K. Magnesium oxychloride cement-based strain-hardening cementitious composite: Mechanical property and water resistance. *Constr. Build. Mater.* **2020**, *261*, 119970. [CrossRef]
25. Wang, Y.; Wei, L.; Yu, J.; Yu, K. Mechanical properties of high ductile magnesium oxychloride cement-based composites after water soaking. *Cem. Concr. Compos.* **2019**, *97*, 248–258. [CrossRef]
26. Chang, C.; An, L.; Lin, R.; Wen, J.; Dong, J.; Zheng, W.; Yan, F.; Xiao, X. Effect of Calcination Temperature on Mechanical Properties of Magnesium Oxychloride Cement. *Materials* **2022**, *15*, 607. [CrossRef]
27. Alghamdi, H.; Shoukry, H.; Perumal, P.; Khawaji, M.; Abadel, A.A. Enhanced mechanical, thermal and fire resistance performance of expanded polystyrene-based fiber-reinforced mortar made with limestone-calcined clay cement (LC3). *Innov. Infrastruct. Solutions* **2023**, *8*, 1–12. [CrossRef]
28. Rawat, S.; Lee, C.; Zhang, Y. Performance of fibre-reinforced cementitious composites at elevated temperatures: A review. *Constr. Build. Mater.* **2021**, *292*, 12338. [CrossRef]
29. Tangirala, A.; Rawat, S.; Lahoti, M. High volume fly ash and basalt-polypropylene fibres as performance enhancers of novel fire-resistant fibre reinforced cementitious composites. *J. Build. Eng.* **2023**, *78*, 107586. [CrossRef]
30. *WB/T1019-2002*; Caustic Burned Magnesia for Magnesium Oxychloride Cement Products. Professional Standard of the People's Republic of China, State Commission for Economic and Trade: Beijing, China, 2002. (In Chinese)
31. Xu, M.; Song, S.; Feng, L.; Zhou, J.; Li, H.; Li, V.C. Development of basalt fiber engineered cementitious composites and its mechanical properties. *Constr. Build. Mater.* **2020**, *266*, 121173. [CrossRef]
32. Missemer, L.; Ouedraogo, E.; Malecot, Y.; Clergue, C.; Rogat, D. Fire spalling of ultra-high performance concrete: From a global analysis to microstructure investigations. *Cem. Concr. Res.* **2018**, *115*, 207–219. [CrossRef]

33. *ASTM C1437*; Standard Test Method for Flow of Hydraulic Cement Mortar. ASTM International: West Conshohocken, PA, USA, 2007.
34. *ASTM C191-21*; Standard Test Methods for Time of Setting of Hydraulic Cement by Vicat Needle. ASTM International: West Conshohocken, PA, USA, 2013.
35. Xia, D.; Chen, R.; Zhang, D.; Cheng, J. Relationship between Fractal Dimension and Properties of Engineered Cementitious Composites with Different Aggregates. *Materials* **2022**, *15*, 7666. [CrossRef]
36. Chen, Z.; Li, J.; Yang, E.-H. Development of Ultra-Lightweight and High Strength Engineered Cementitious Composites. *J. Compos. Sci.* **2021**, *5*, 113. [CrossRef]
37. Blazy, J.; Blazy, R. Polypropylene fiber reinforced concrete and its application in creating architectural forms of public spaces. *Case Stud. Constr. Mater.* **2021**, *14*, e00549. [CrossRef]
38. Noumowe, A. Mechanical properties and microstructure of high strength concrete containing polypropylene fibres exposed to temperatures up to 200 °C. *Cem. Concr. Res.* **2005**, *35*, 2192–2198. [CrossRef]
39. Akca, A.H.; Zihnioğlu, N. High performance concrete under elevated temperatures. *Constr. Build. Mater.* **2013**, *44*, 317–328. [CrossRef]